

Identification of dipole disorder in low temperature solution processed oxides: Its utility and suppression for transparent high performance solution-processed hybrid electronics.

Kulbinder Banger,^{1*} Christopher Warwick,^{1‡} Jiang Lang,^{1‡} Katharina Broch,^{1‡} Jonathan Halpert,¹ Josephine Socratous,¹ Adam Brown,¹ Timothy Leedham,^{2†} Henning Sirringhaus^{1*}

1. Optoelectronics Group, Cavendish Laboratory, JJ Thomson Avenue, Cambridge CB3 0HE, United Kingdom.
2. Multivalent Ltd., Eriswell, Suffolk IP27 9BJ, United Kingdom.

[†] posthumous (November 2013)

[‡] equal contribution

^{*} corresponding authors

Supporting Info:

Figure S1: Electrical device characterization for solution processed IZO (7:3 oxide ratio) TFTs annealed at 225 °C for 2h on ALD grown Al₂O₃, (150 °C, thickness 100nm). **a)** Transfer curve at V_{DS} = 1 & 5V, W/L =10, **b)** output curve, Vg 0-30V step 5V. **c)** Constant current stress measurements (5μA); ΔVt after 50,000 s = 0.9 V, **d)** tabulation of TFT parameters.

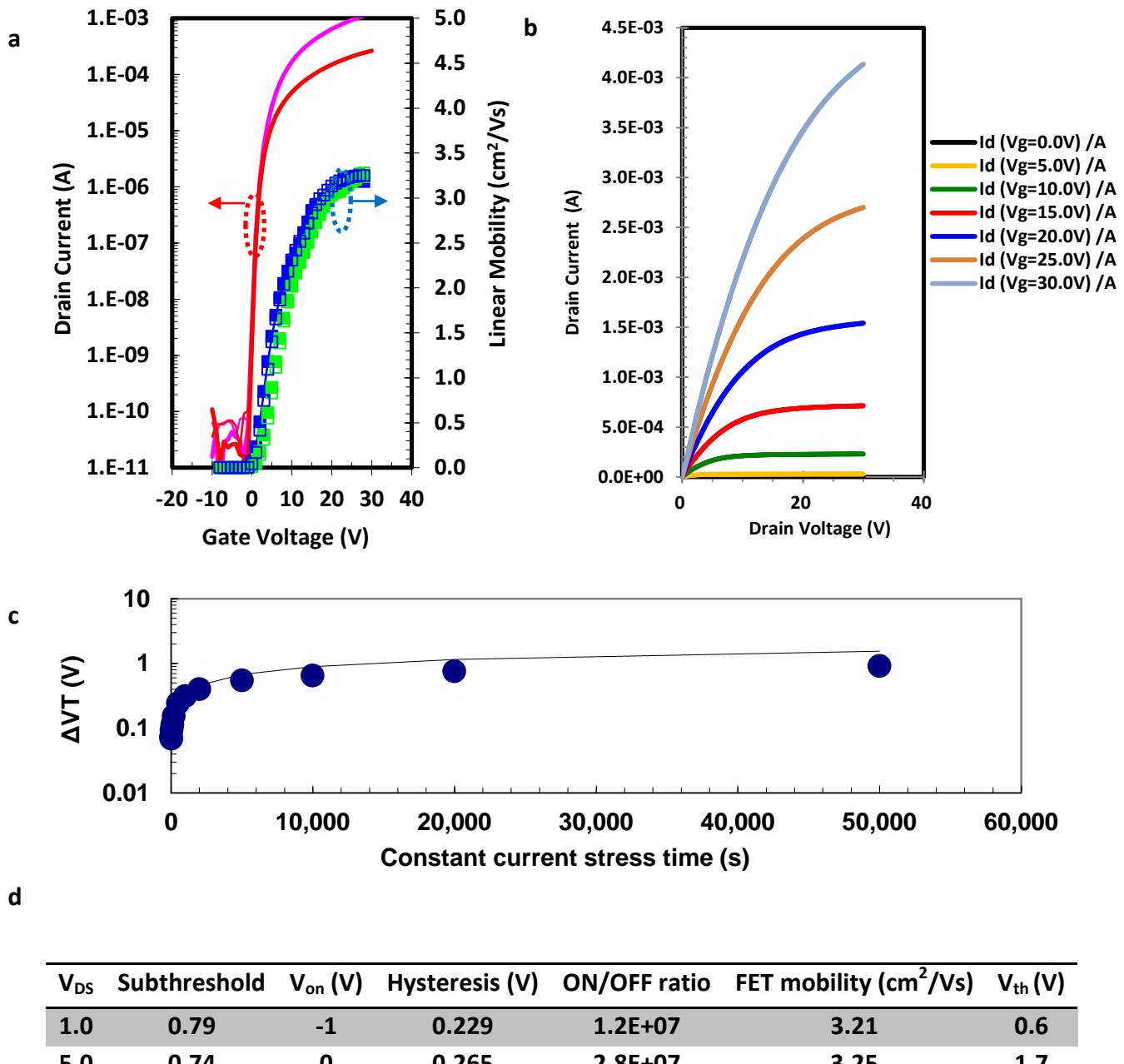


Figure S2 Electrical device characterization for solution processed IZO (7:3 oxide ratio) TFTs annealed at 225 °C for 2h on SiO₂ (thickness 100nm). **a)** transfer curve at V_{DS} = 2 & 5V, W/L =10 , **b)** output curve, Vg 0-40V step 5V. **c)** Constant current stress measurements (5μA); ΔVt after 50,000 s = 1.7 V, **d)** tabulation of TFT parameters.

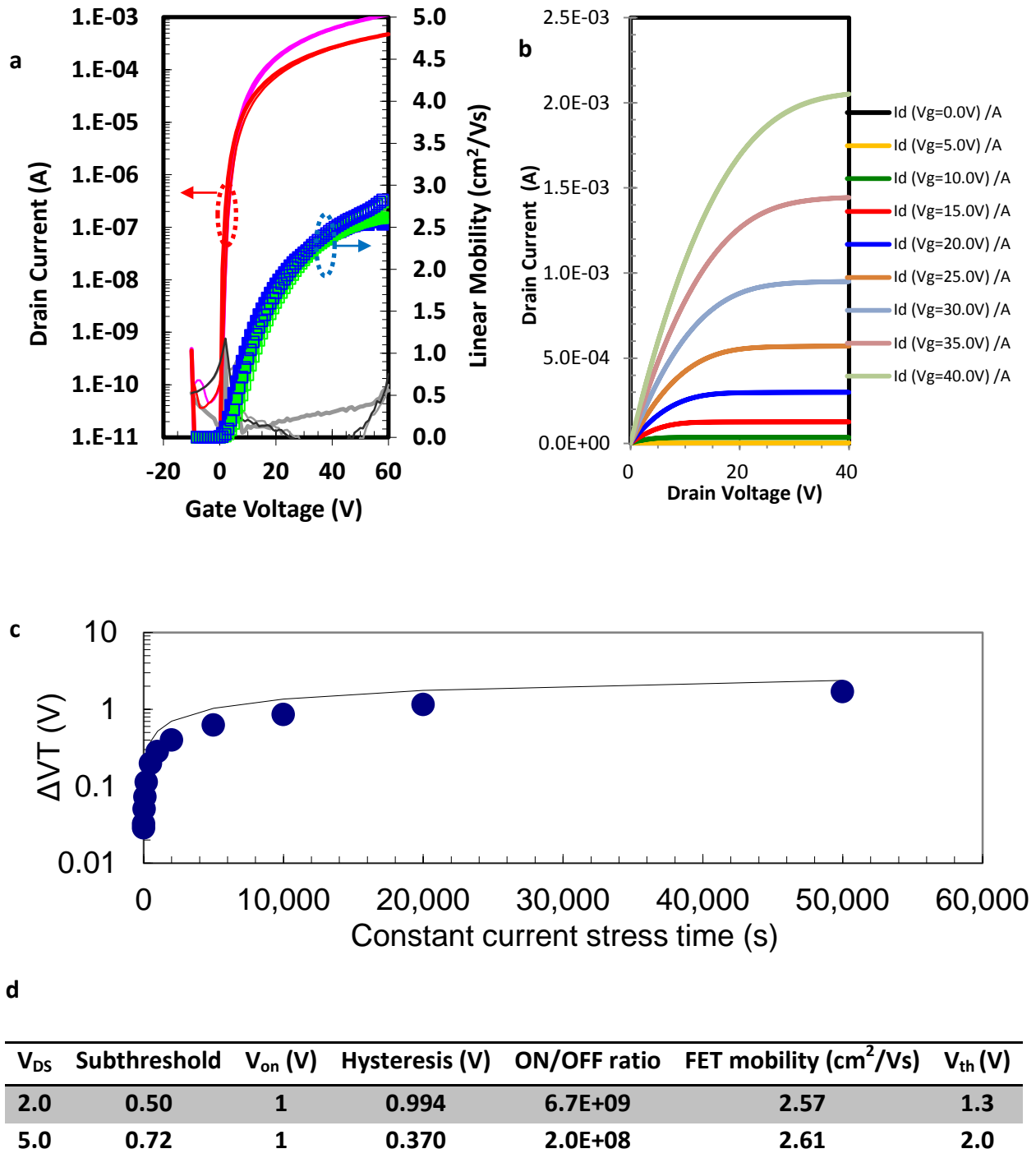


Figure S3. Impedance analysis characterization on Metal-Insulator-Metal Structures (MIM) for reference ALD grown, and solution processed alumina. **a)** Capacitance versus frequency measurements (+5V) and **b)** current density versus electric field plots for reference ALD grown Al_2O_3 from $[\text{AlOCCH}(\text{CH}_3)_2]_n$ at 150°C , thickness 100 nm, radius = 250 μm ; **c)** Capacitance versus frequency measurements (+5V) and **d)** current density versus electric field plots for solution processed alumina sample grown from 0.3M solution of $[\text{AlOCCH}(\text{CH}_3)_2]_n$ in Isopropanol, annealed at 300°C , thickness 75nm, radius = 250 μm ; **e)** AFM measurements for alumina fabricated via (left) ALD and (right) spin coating.

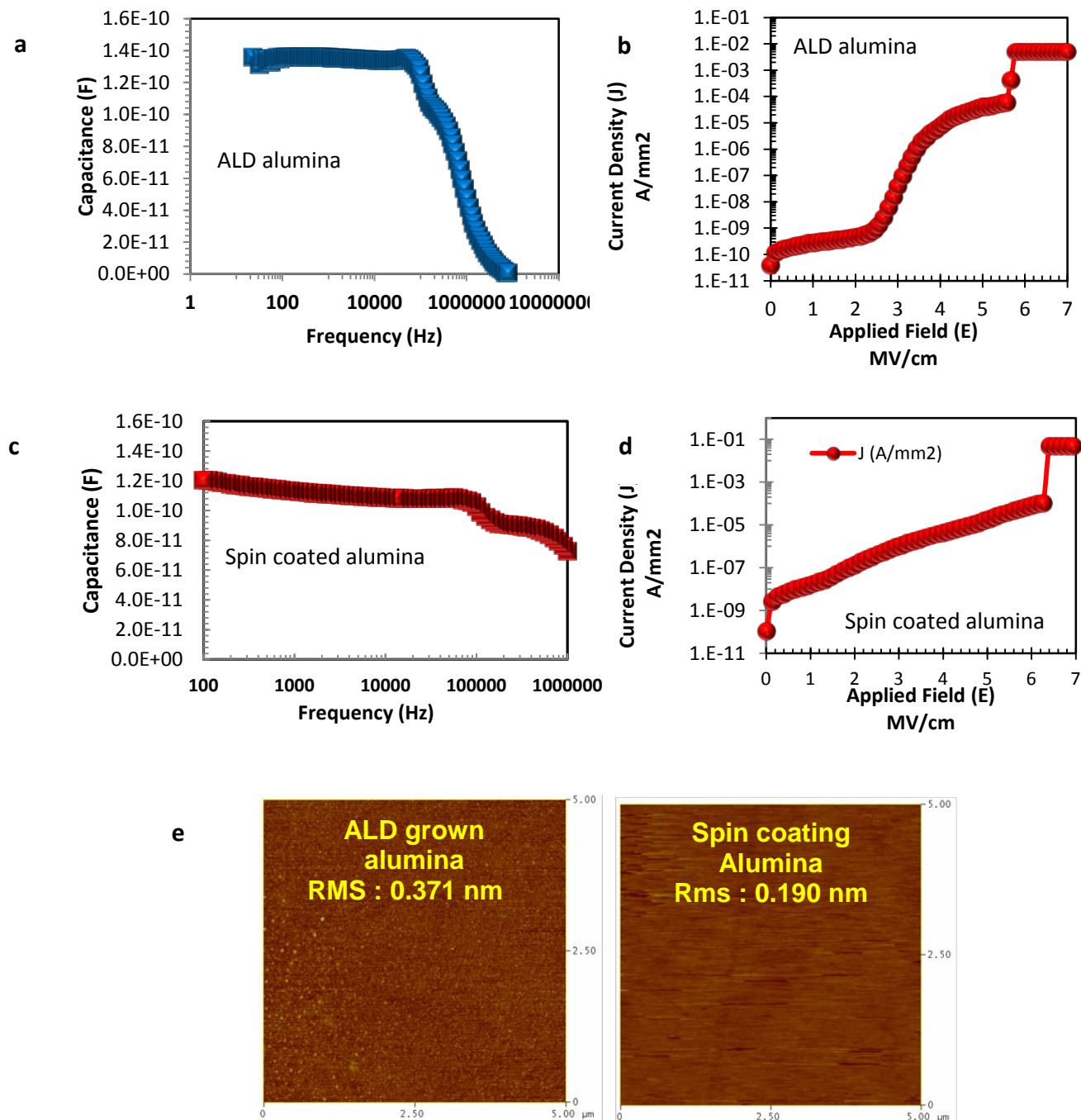
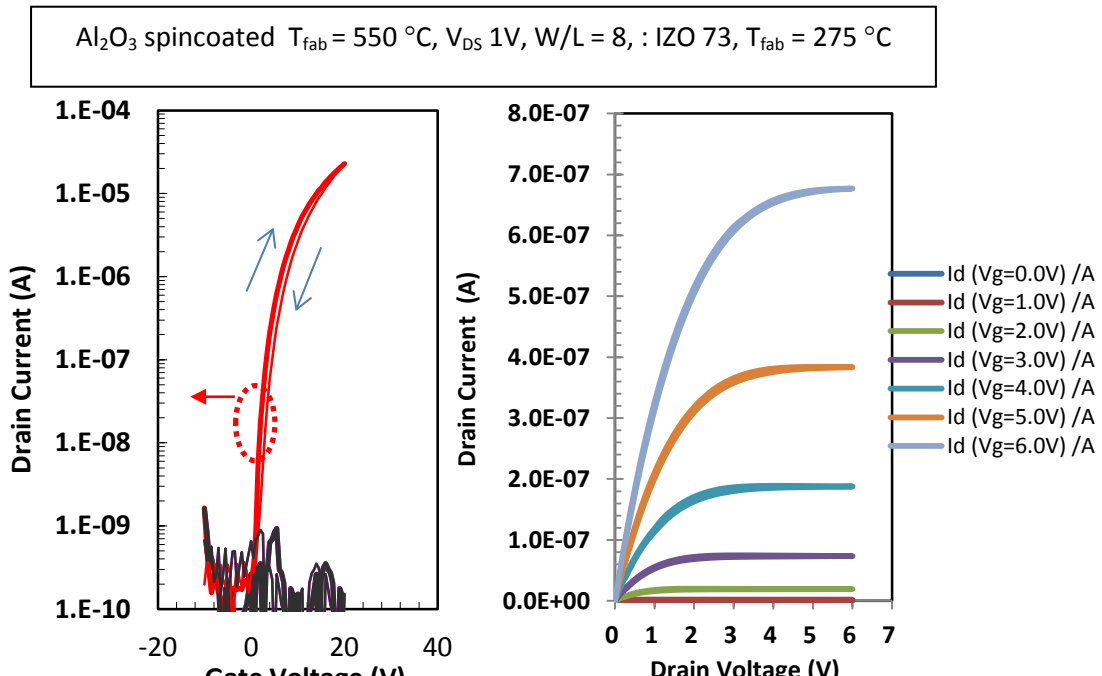
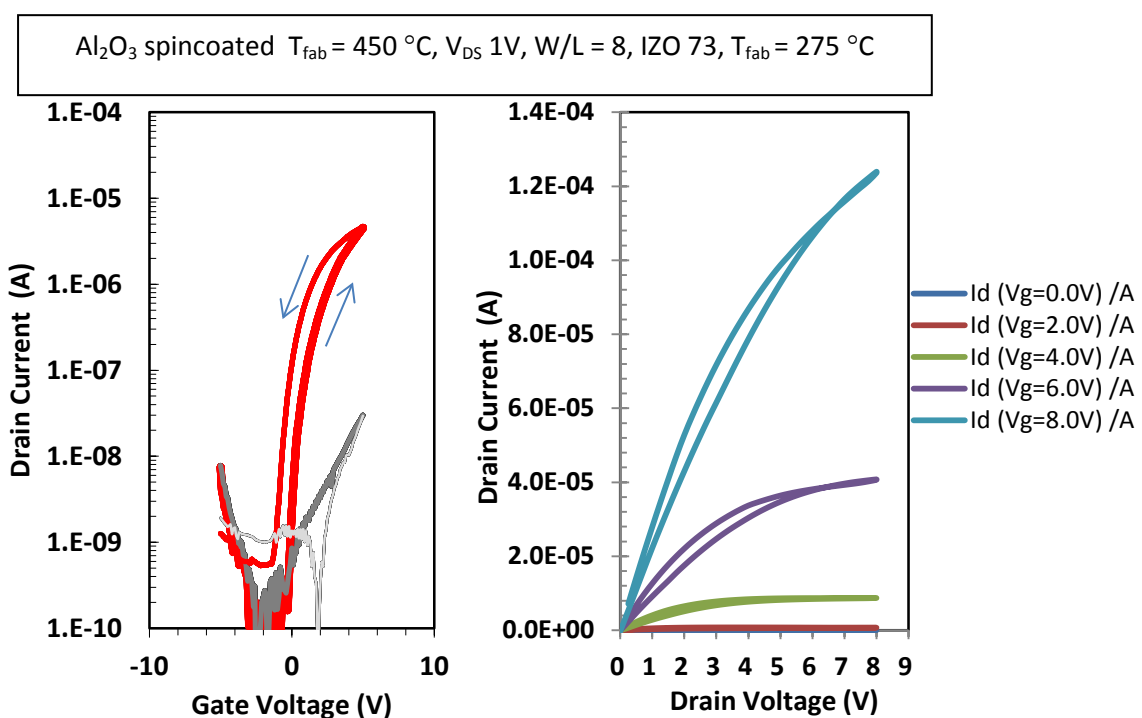


Figure S4. Hysteresis observed in transfer and output curves for solution processed IZO TFTs on solution processed alumina annealed at different temperatures. In all cases, solution processed InZnO (7:3 oxide ratio) annealed at 275 °C for 2h on pre-fabricated solution processed Al₂O₃ from 0.3M solution of [AlOCCH(CH₃)₂]_n in Isopropanol. Tungsten source and drain contacts (40-50nm) were sputter deposited via shadow mask. **a)** TFT transfer curves of BGTC solution spun Al₂O₃ annealed at 550 °C, apparent $\mu=1.25 \text{ cm}^2\text{Vs}^{-1}$ **b)** TFT transfer curves of BGTC solution spun Al₂O₃ annealed at 450 °C apparent $\mu=3.61 \text{ cm}^2\text{Vs}^{-1}$ **c)** TFT transfer curves of BGTC solution spun Al₂O₃ annealed at 350 °C apparent $\mu=19.5 \text{ cm}^2\text{Vs}^{-1}$; **d)** TFT transfer curves of BGTC solution spun Al₂O₃ annealed at 300 °C, and IZO (oxide ratio 7:3) annealed at 275 °C for 2hrs, (red = Id, Blue = mobility), measured in continuous mode and in pulsed mode with varying magnitude of rest voltage demonstrating removal of hysteresis when gate voltage is biased at sufficiently large negative voltage (OFF state).

a



b



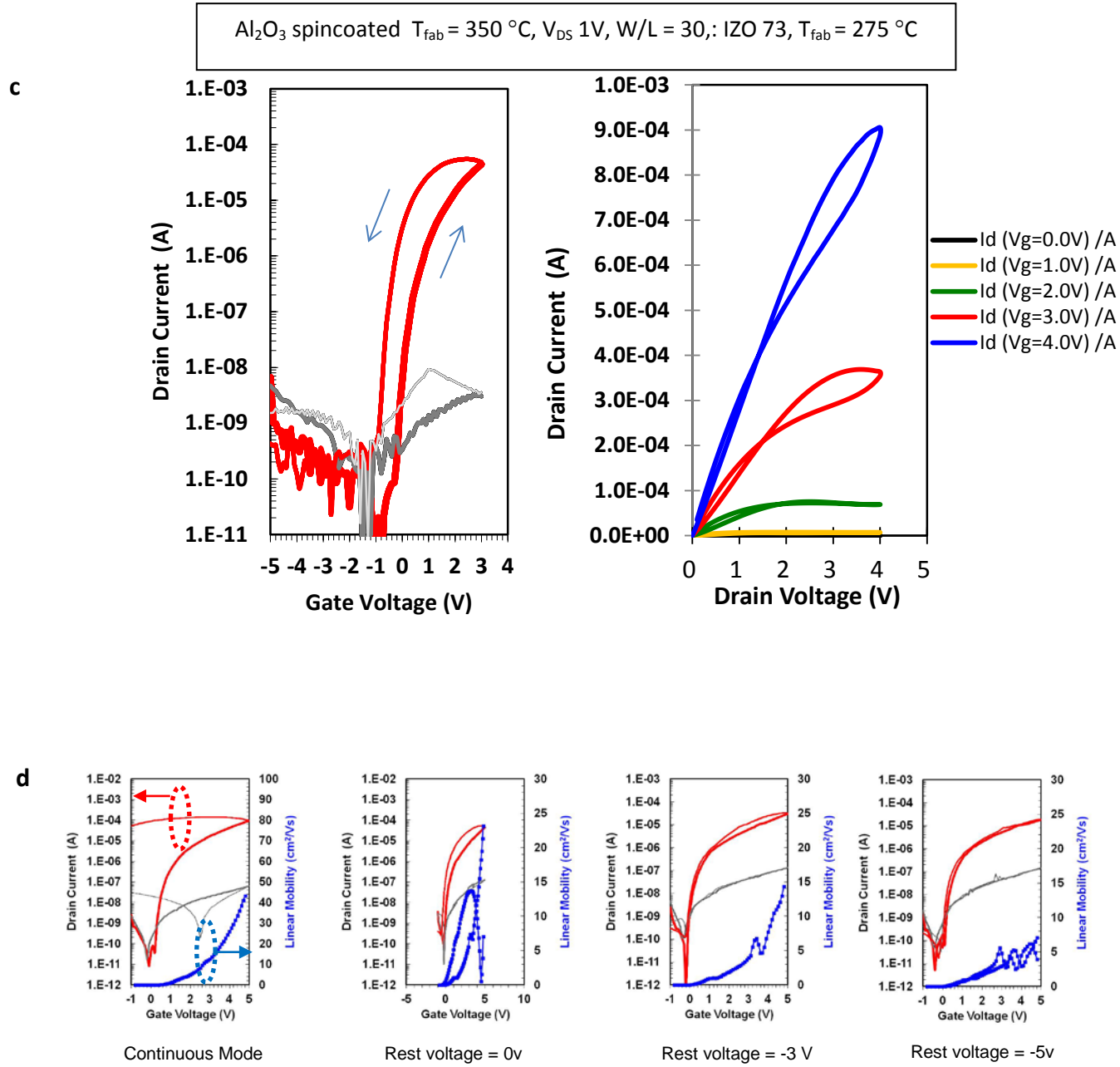


Figure S5: Evidence of induced dipole in other solution processed materials systems **a)** Zr (film thickness 236-218 nm), and **b)** Hf oxide films (film thickness of 286- 158nm annealed at 275-450 °C respectively) deposited from molecular alkoxides ($M_x(OCH(CH_3)_2)_y$] precursor inks showing conductance and permittivity values as a function of frequency and process temperature.

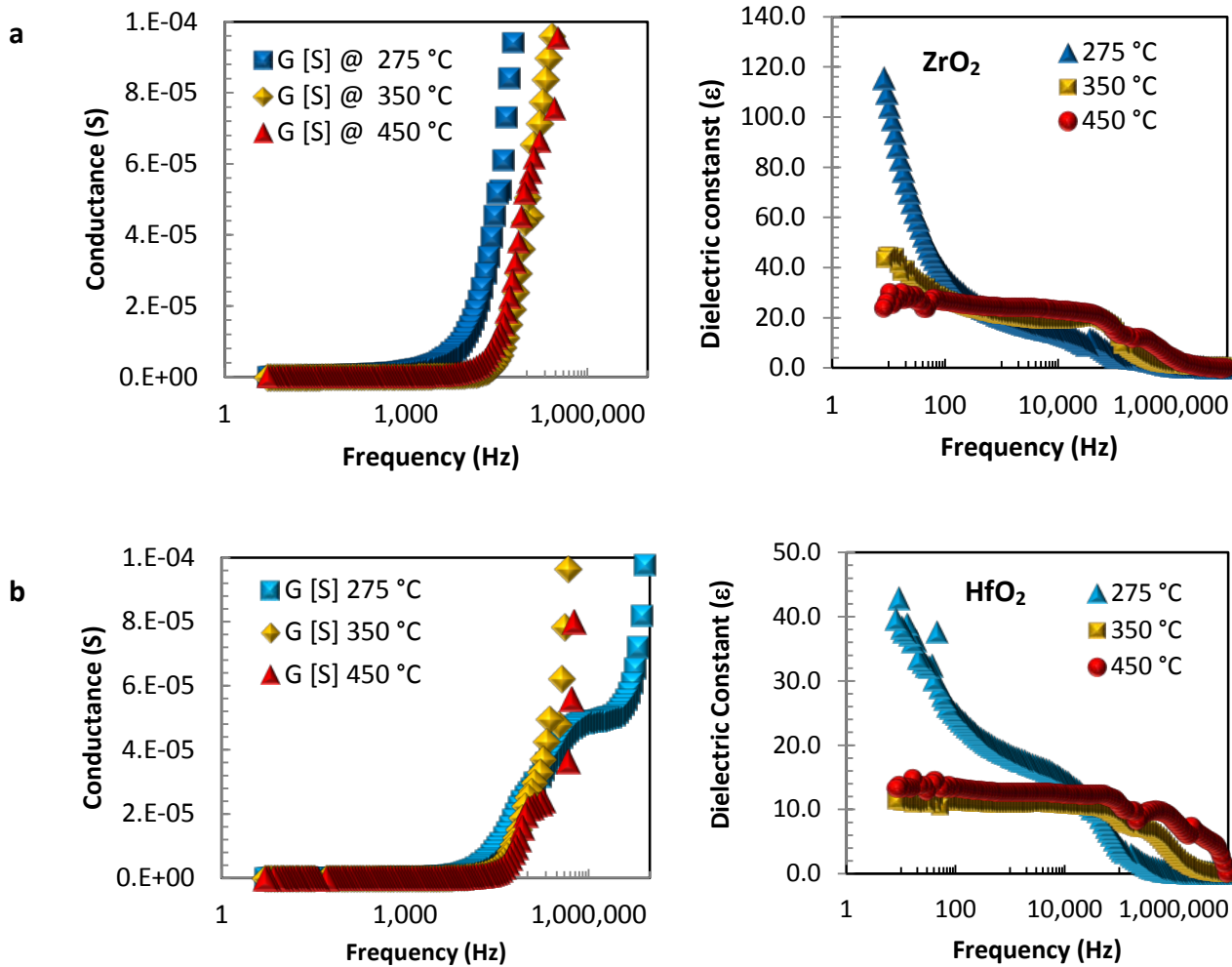


Figure S6: ZrO₂ dielectric layers (93-138nm) spincoated from ZrOCl₂ oxyhalide precursor dissolved in high purity HPLC grade 2-methoxyethanol. **a)** Conductance and **b)** permittivity response as a function of frequency and annealing temperature, **c)** BGTC TFT transfer (left) and output (right) characteristics for IZO (7:3 oxide ratio), W/L 3000/200μm, V_{DS} 1,5 V TFTs processed at 275 °C using a solution processed ZrO₂ layer (thickness 100nm, annealed at 350 °C, $\epsilon=14$ extrapolated to 1Hz (see S6b), V_{DS} = 1, 5 V in the transfer characteristics) **d)** Respective constant current bias stress data for the TFT device (5 μA over 14h, $\Delta V_t = 4.98$ V).

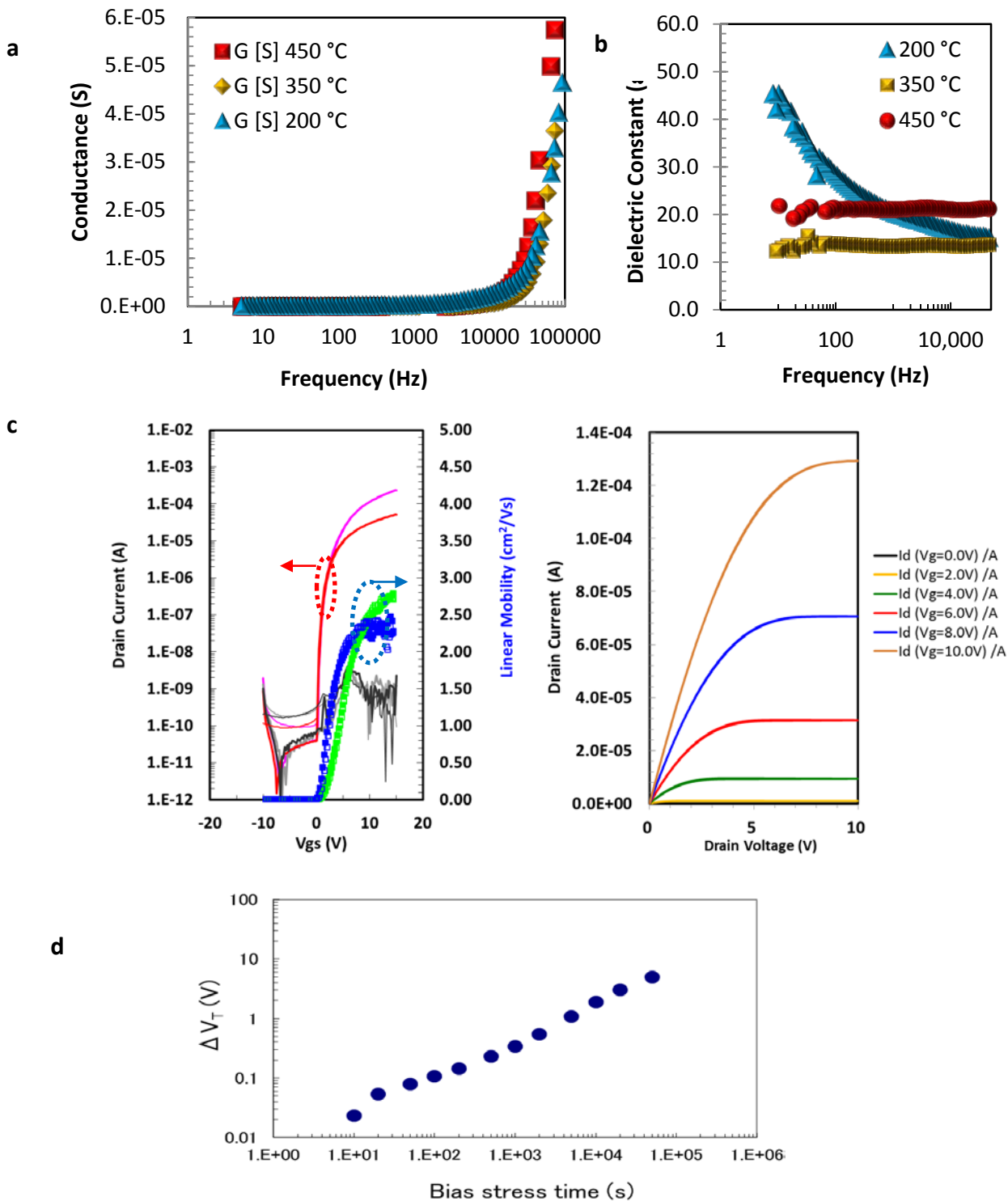
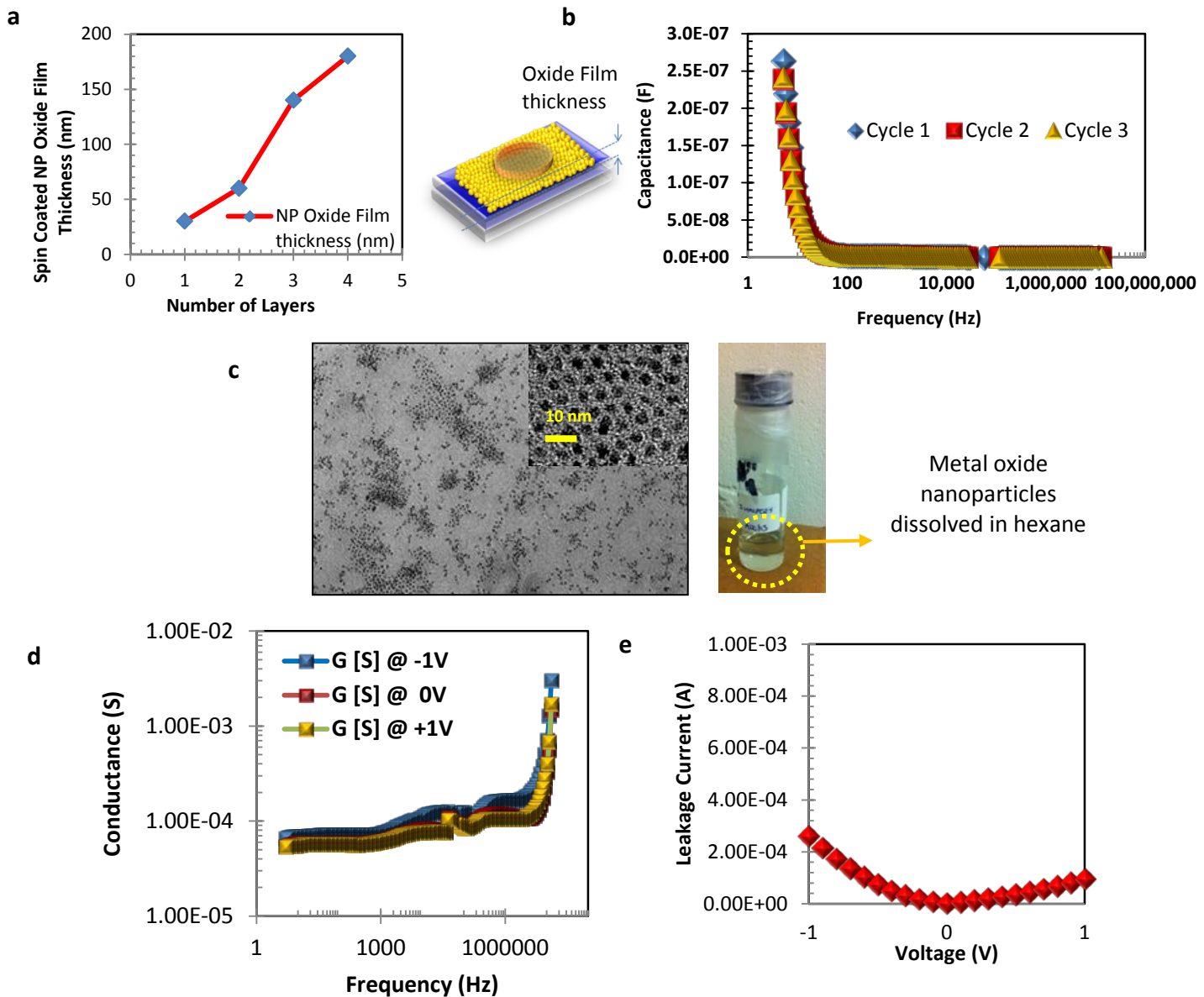


Figure S7 Solution processed HfZrO_x thin film dielectric layer fabricated from a nanoparticle based ink in hexane.¹ Devices were annealed at 90 °C between coatings to achieve a final film thickness of 175nm and then fully annealed at 200 °C for 60 minutes before depositing an Al top electrode (50nm thickness, radius 125μm) to complete the MIM device structure. **a)** film thickness vs number of layers, **b)** capacitance vs frequency dependence **c)** TEM image of TOPO capped oxide nanoparticles showing excellent dispersion. **d)** conductance vs frequency plot **e)** leakage current measurements vs applied voltage.



1. Livage, J., Beteille, F., Roux, C., Chatry, M. & Davidson, *Acta Mater.* **46**, 743–750 (1998).

Capacitance vs Frequency performance for thin films processed at 200 °C, recorded extremely high relative permittivity of $\epsilon_r \sim 35,000$, with areal capacitance of $492 \mu\text{Fcm}^{-2}$, 28.1 Fcm^{-3} corresponding to a volumetric energy density of $3.5 \times 10^{-2} \text{ Wh cm}^{-3}$ and 126.46 W cm^{-3} respectively. These values compare well to super capacitors which consist of materials with very high surface area such as reduced graphene oxide (RGO) and aerogels with ideal values for specific energy are 10^{-3} to $10^{-2} \text{ Wh cm}^{-3}$ and power $10^{+2} - 10^{+3} \text{ Wcm}^{-3}$.^{2,3} Cycling the device through repeated measurements show limited decline of $0.02 \mu\text{F}$, thus our nanoparticle oxides based capacitors, although unsuitable for TFT's may be utilized for energy storage.⁴

2. M. F. El-Kady and R. B. Kaner, Nat. Commun., 2013, 4, 1475.

3. Z.-S. Wu, K. Parvez, X. Feng and K. Müllen, Nat. Commun., 2013, 4, 2487

4. Y. Gogotsi and P. Simon, Science, 2011, 334, 917–8.

Figure S8: Permittivity vs frequency plots of MIM devices (top contact Al thickness 50nm, radius = 250 μ m) for Alumina layers (thickness ALD = 60 nm spincoated 80-100 nm), spin coated from high purity $\text{Al}(\text{NO}_3)_3$ (99.999 %) dissolved in 2-methoxyethanol under different annealing conditions.

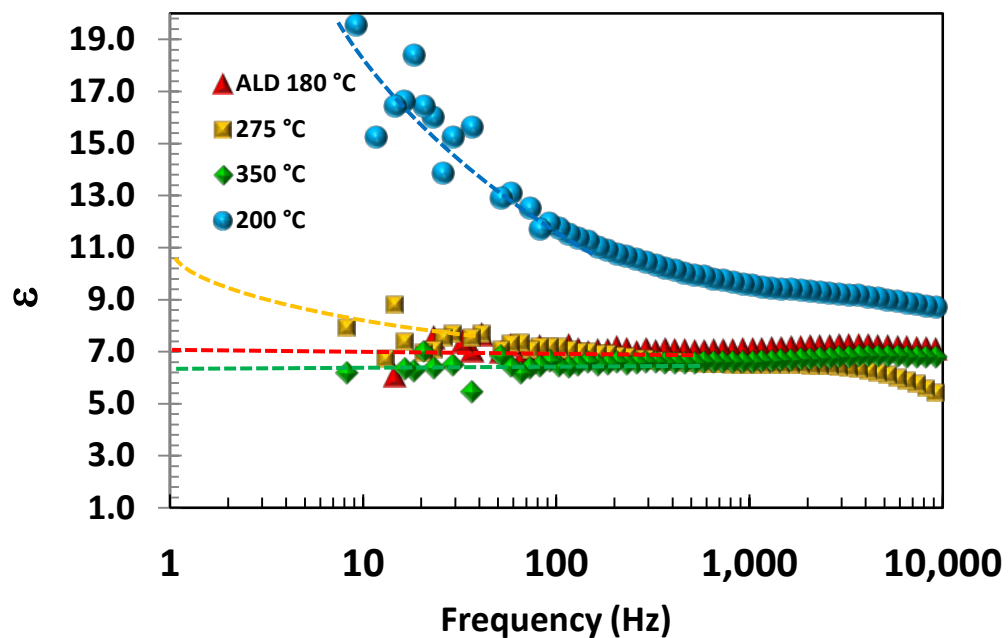


Figure S9 Chemical analysis of solution processed alumina layers. **a)** REELS analysis: Band to band transition show defined bang gap (E_g) transition at 7.5 and 6.8eV for ALD and spincoated Al_2O_3 respectively (see arrows below). Energy loss peak at $\sim 2\text{eV}$ is due to electrons elastically scattered from hydrogen. The measurements reveal a higher concentration of hydrogen in spin coated alumina films compared to ALD grown alumina. **b)** Table showing XPS compositional analysis for solution processed Alumina at various annealing temperatures compared to a reference ALD Alumina sample grown at 150 °C

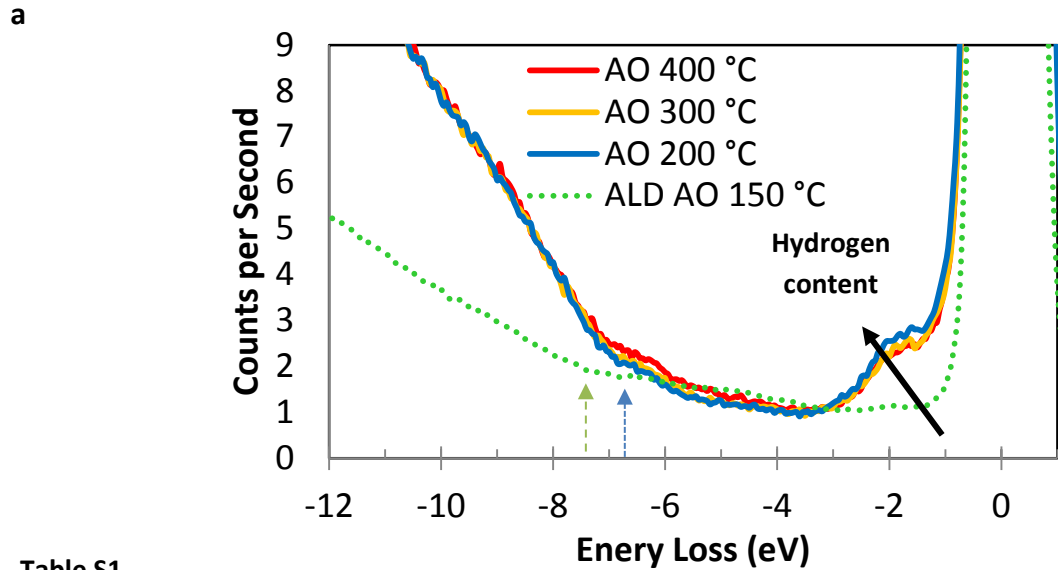
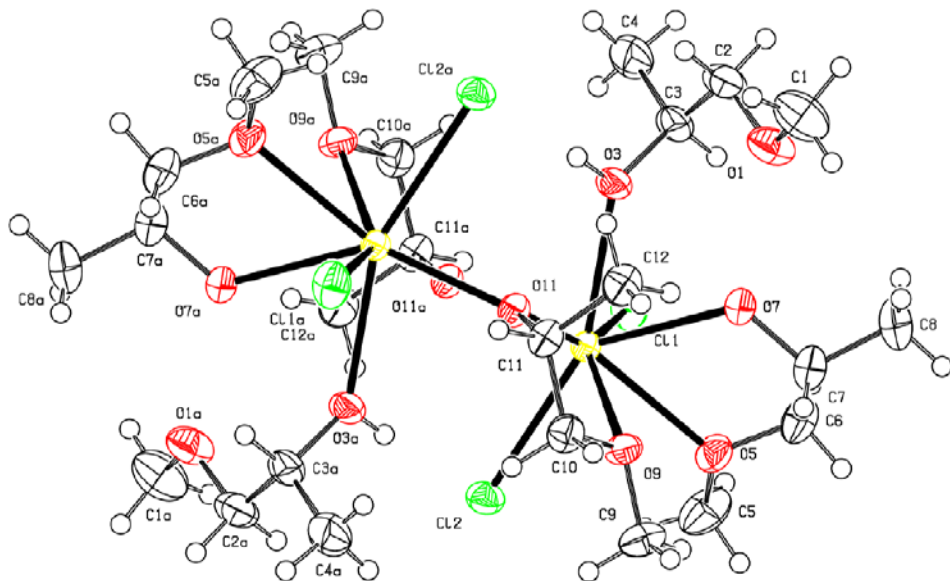


Table S1

Sample		M-OH	M-Ovac	M-Olattice	Al 2p
ALD AO 150 °C	BE eV	531.53	530.75	529.93	73.55
REF	FWHM	1.85	1.7	2.11	1.88
	% area	3.33	11.72	44.90	40.04
		M-OH	M-Ovac	M-Olattice	Al 2p
AO 400 °C	BE eV	531.46	530.23	529.01	75.52
	FWHM	1.56	1.69	1.86	1.84
	% area	5.56	18.84	36.76	38.81
		M-OH	M-Ovac	M-Olattice	Al 2p
AO 300 °C	BE eV	531.28	530.12	528.99	75.48
	FWHM	1.65	1.79	1.84	1.84
	% area	6.99	22.64	32.09	38.28
		M-OH	M-Ovac	M-Olattice	Al 2p
AO 200 °C	BE eV	531.04	530.03	528.94	72.45
	FWHM	1.54	1.76	1.88	1.82
	% area	9.42	24.31	29.30	36.98

Figure S10: Single crystal data and structure refinement for $\text{La}_2(\text{C}_{24}\text{H}_{56}\text{O}_{12})\text{Cl}_4$.

Identification code	kk1401
Empirical formula	$\text{C}_{24}\text{H}_{56}\text{Cl}_4\text{La}_2\text{O}_{12}$
Formula weight	956.31
Temperature	180(2) K
Wavelength	0.71073 Å
Crystal system	Monoclinic
Space group	P2(1)/n
Unit cell dimensions	 a = 11.3100(2) Å $\alpha = 90^\circ$. b = 10.2958(2) Å $\beta = 95.490(1)^\circ$. c = 17.6004(3) Å $\gamma = 90^\circ$.
Volume	2040.09(6) Å ³
Z	2
Density (calculated)	1.557 Mg/m ³
Absorption coefficient	2.374 mm ⁻¹
F(000)	956
Crystal size	0.18 x 0.18 x 0.14 mm ³
Theta range for data collection	3.62 to 33.75°.
Index ranges	-17 <= h <= 17, -15 <= k <= 15, -27 <= l <= 27
Reflections collected	18515
Independent reflections	8079 [R(int) = 0.0357]
Completeness to theta = 33.75°	99.0 %
Absorption correction	Semi-empirical from equivalents
Max. and min. transmission	0.754 and 0.629
Refinement method	Full-matrix least-squares on F ²
Data / restraints / parameters	8079 / 1 / 199
Goodness-of-fit on F ²	0.963
Final R indices [I > 2sigma(I)]	R1 = 0.0259, wR2 = 0.0548
R indices (all data)	R1 = 0.0467, wR2 = 0.0564
Largest diff. peak and hole	1.023 and -0.811 e.Å ⁻³



Bond lengths [Å] and angles [°] for kk1401

Bond (A-B)	Length Å	Bond (A-B)	Length Å
La(1)-O(11)	2.3859(13)	C(5)-H(5A)	0.9800
La(1)-O(11)#1	2.4144(13)	C(5)-H(5B)	0.9800
La(1)-O(7)	2.5723(14)	C(5)-H(5C)	0.9800
La(1)-O(3)	2.5773(15)	C(6)-C(7)	1.481(4)
La(1)-O(5)	2.6678(14)	C(6)-H(6A)	0.9900
La(1)-O(9)	2.7222(14)	C(6)-H(6B)	0.9900
La(1)-Cl(1)	2.8152(6)	O(7)-C(7)	1.445(3)
La(1)-Cl(2)	2.8620(5)	C(7)-C(8)	1.501(3)
La(1)-La(1)#1	3.9627(2)	C(7)-H(7)	1.0000
O(1)-C(1)	1.421(3)	C(8)-H(8A)	0.9800
O(1)-C(2)	1.431(3)	C(8)-H(8B)	0.9800
C(1)-H(1A)	0.9800	C(8)-H(8C)	0.9800
C(1)-H(1B)	0.9800	O(9)-C(9)	1.438(2)
C(1)-H(1C)	0.9800	O(9)-C(10)	1.440(3)
C(2)-C(3)	1.500(3)	C(9)-H(9A)	0.9800
C(2)-H(2A)	0.9900	C(9)-H(9B)	0.9800
C(2)-H(2B)	0.9900	C(9)-H(9C)	0.9800
O(3)-C(3)	1.429(3)	C(10)-C(11)	1.516(3)
O(3)-H(3A)	0.87(2)	C(10)-H(10A)	0.9900
C(3)-C(4)	1.519(3)	C(10)-H(10B)	0.9900
C(3)-H(3)	1.0000	O(11)-C(11)	1.422(2)
C(4)-H(4A)	0.9800	O(11)-La(1)#1	2.4144(13)
C(4)-H(4B)	0.9800	C(11)-C(12)	1.517(3)
C(4)-H(4C)	0.9800	C(11)-H(11)	1.0000
O(5)-C(6)	1.424(3)	C(12)-H(12A)	0.9800
O(5)-C(5)	1.438(3)	C(12)-H(12B)	0.9800

Bond Group (A-B-C)	Angle °	Bond Group (A-B-C)	Angle °
O(11)-La(1)-O(11)#1	68.72(5)	O(7)-La(1)-O(9)	74.07(5)
O(11)-La(1)-O(7)	98.16(5)	O(3)-La(1)-O(9)	117.90(5)
O(11)#1-La(1)-O(7)	141.07(5)	O(5)-La(1)-O(9)	69.89(5)
O(11)-La(1)-O(3)	76.73(5)	O(11)-La(1)-Cl(1)	150.26(3)
O(11)#1-La(1)-O(3)	75.93(5)	O(11)#1-La(1)-Cl(1)	87.61(3)
O(7)-La(1)-O(3)	65.28(5)	O(7)-La(1)-Cl(1)	89.02(4)
O(11)-La(1)-O(5)	133.87(5)	O(3)-La(1)-Cl(1)	80.30(4)
O(11)#1-La(1)-O(5)	152.20(5)	O(5)-La(1)-Cl(1)	74.61(4)
O(9)-La(1)-Cl(1)	144.49(3)	O(9)-La(1)-La(1)#1	95.27(3)
O(11)-La(1)-Cl(2)	94.16(3)	Cl(1)-La(1)-La(1)#1	119.824(13)
O(11)#1-La(1)-Cl(2)	80.32(3)	Cl(2)-La(1)-La(1)#1	86.629(11)
O(7)-La(1)-Cl(2)	138.37(3)	C(1)-O(1)-C(2)	112.9(2)
O(3)-La(1)-Cl(2)	156.23(4)	O(1)-C(1)-H(1A)	109.5
O(5)-La(1)-Cl(2)	81.74(4)	O(1)-C(1)-H(1B)	109.5
O(9)-La(1)-Cl(2)	75.81(3)	H(1A)-C(1)-H(1B)	109.5
Cl(1)-La(1)-Cl(2)	99.467(18)	O(1)-C(1)-H(1C)	109.5
O(11)-La(1)-La(1)#1	34.59(3)	H(1A)-C(1)-H(1C)	109.5
O(11)#1-La(1)-La(1)#1	34.13(3)	H(1B)-C(1)-H(1C)	109.5
O(7)-La(1)-La(1)#1	124.02(3)	O(1)-C(2)-C(3)	109.46(19)
O(3)-La(1)-La(1)#1	73.36(3)	O(1)-C(2)-H(2A)	109.8

O(5)-La(1)-La(1)#1	162.98(4)	C(3)-C(2)-H(2A)	109.8
O(1)-C(2)-H(2B)	109.8	C(7)-C(6)-H(6B)	109.8
C(3)-C(2)-H(2B)	109.8	H(6A)-C(6)-H(6B)	108.2
H(2A)-C(2)-H(2B)	108.2	C(7)-O(7)-La(1)	122.21(13)
C(3)-O(3)-La(1)	135.73(14)	O(7)-C(7)-C(6)	107.9(2)
C(3)-O(3)-H(3A)	109.9(17)	O(7)-C(7)-C(8)	111.4(2)
La(1)-O(3)-H(3A)	114.3(17)	C(6)-C(7)-C(8)	114.7(2)
O(3)-C(3)-C(2)	110.3(2)	O(7)-C(7)-H(7)	107.5
O(3)-C(3)-C(4)	111.64(19)	C(6)-C(7)-H(7)	107.5
C(2)-C(3)-C(4)	111.3(2)	C(8)-C(7)-H(7)	107.5
O(3)-C(3)-H(3)	107.8	C(7)-C(8)-H(8A)	109.5
C(2)-C(3)-H(3)	107.8	C(7)-C(8)-H(8B)	109.5
C(4)-C(3)-H(3)	107.8	H(8A)-C(8)-H(8B)	109.5
C(3)-C(4)-H(4A)	109.5	C(7)-C(8)-H(8C)	109.5
C(3)-C(4)-H(4B)	109.5	H(8A)-C(8)-H(8C)	109.5
H(4A)-C(4)-H(4B)	109.5	H(8B)-C(8)-H(8C)	109.5
C(3)-C(4)-H(4C)	109.5	C(9)-O(9)-C(10)	110.12(16)
H(4A)-C(4)-H(4C)	109.5	C(9)-O(9)-La(1)	124.37(12)
H(4B)-C(4)-H(4C)	109.5	C(10)-O(9)-La(1)	111.46(11)
C(6)-O(5)-C(5)	110.42(18)	O(9)-C(9)-H(9A)	109.5
C(6)-O(5)-La(1)	117.45(13)	O(9)-C(9)-H(9B)	109.5
C(5)-O(5)-La(1)	119.88(14)	H(9A)-C(9)-H(9B)	109.5
O(5)-C(5)-H(5A)	109.5	O(9)-C(9)-H(9C)	109.5
O(5)-C(5)-H(5B)	109.5	H(9A)-C(9)-H(9C)	109.5
H(5A)-C(5)-H(5B)	109.5	H(9B)-C(9)-H(9C)	109.5
O(5)-C(5)-H(5C)	109.5	O(9)-C(10)-C(11)	109.15(17)
H(5A)-C(5)-H(5C)	109.5	O(9)-C(10)-H(10A)	109.9
H(5B)-C(5)-H(5C)	109.5	C(11)-C(10)-H(10A)	109.9
O(5)-C(6)-C(7)	109.6(2)	O(9)-C(10)-H(10B)	109.9
O(5)-C(6)-H(6A)	109.8	C(11)-C(10)-H(10B)	109.9
C(7)-C(6)-H(6A)	109.8	H(10A)-C(10)-H(10B)	108.3
C(11)-O(11)-La(1)	121.70(11)	C(12)-C(11)-H(11)	107.8
C(11)-O(11)-La(1)#1	126.24(11)	C(11)-C(12)-H(12A)	109.5
La(1)-O(11)-La(1)#1	111.28(5)	C(11)-C(12)-H(12B)	109.5
O(11)-C(11)-C(10)	109.14(16)	H(12A)-C(12)-H(12B)	109.5
O(11)-C(11)-C(12)	111.42(18)	C(11)-C(12)-H(12C)	109.5
C(10)-C(11)-C(12)	112.61(18)	H(12A)-C(12)-H(12C)	109.5
O(11)-C(11)-H(11)	107.8	H(12B)-C(12)-H(12C)	109.5
C(10)-C(11)-H(11)	107.8		

Symmetry transformations used to generate equivalent atoms:

#1 -x+2,-y,-z+1

Figure S11 Dielectric constant vs frequency plot for MIM device (radius 250 μm , thickness 83- 69nm for 200 to 450 $^{\circ}\text{C}$ respectively) for solution processed Al_2O_3 doped with La 12.5 at% annealed at different temperatures.

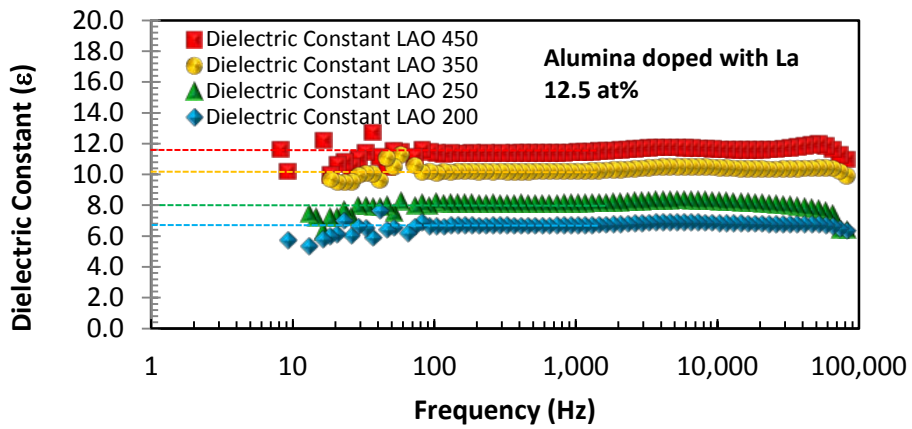


Figure S12. XRD analysis for solution processed La doped alumna films on Si(100) wafer. (Diffraction peaks labelled * are from the underlying Si substrate).

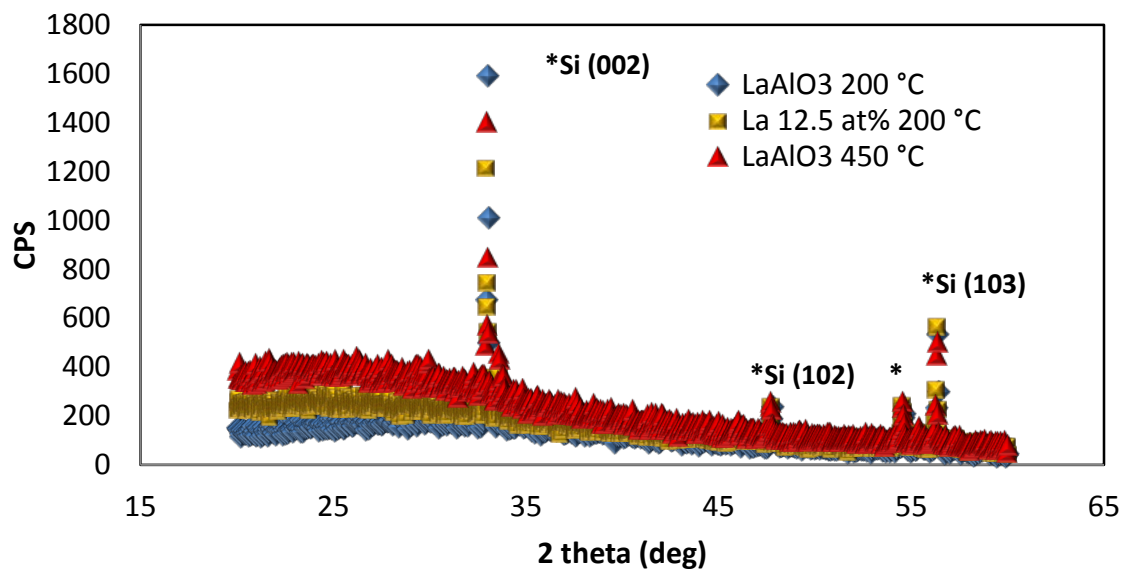


Figure S13 Morphological analysis of solution processed LaAlO₃ annealed at 200 °C. **a)** SEM image ‘edge-on’, **b)** AFM images showing a surface roughness of 0.2 nm; **c)** ellipsometry based Cauchy fit for transparent LaAlO₃ oxide layer, the inset shows the real and imaginary part of the extracted refractive index.

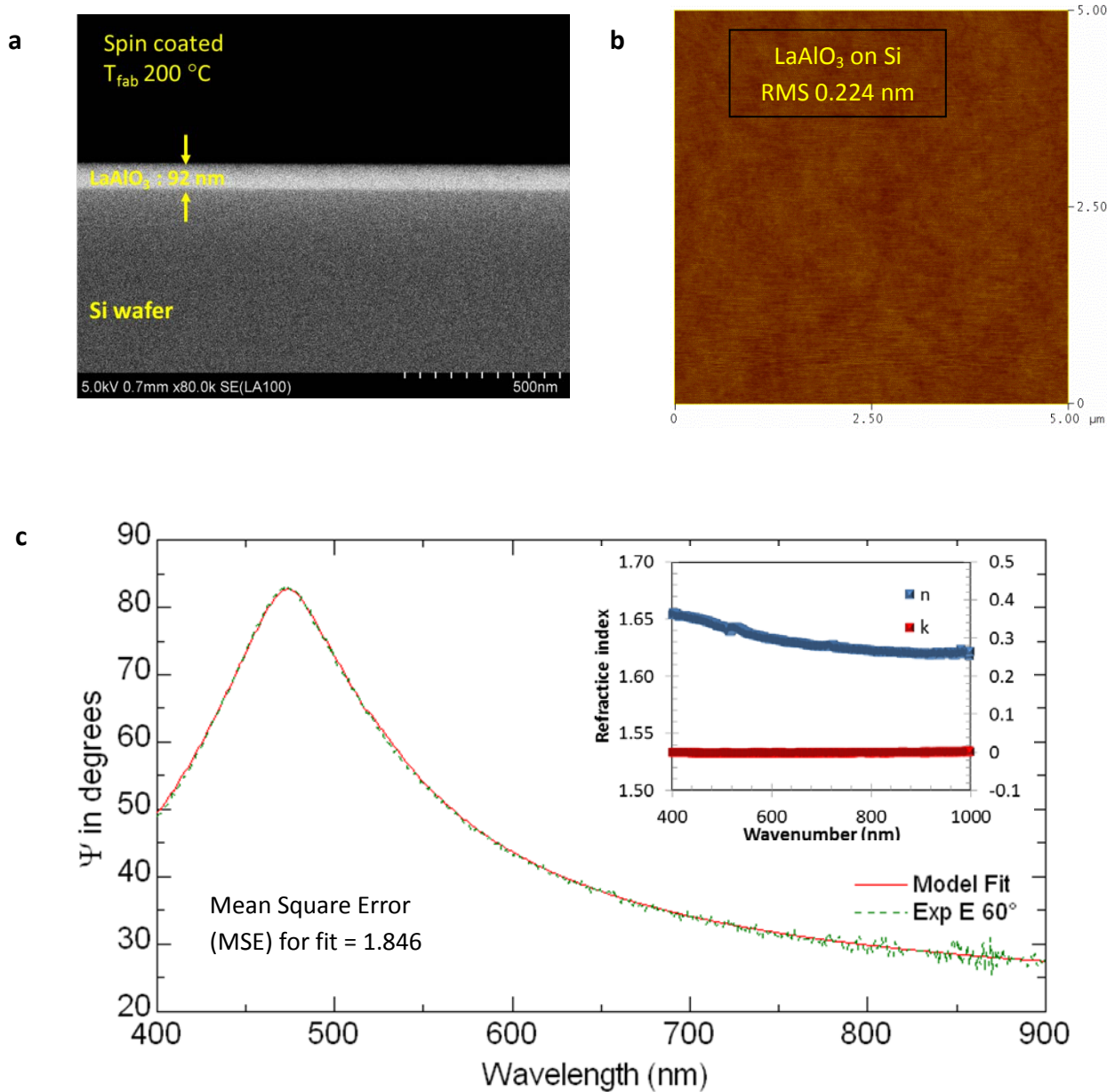


Figure S14: Dielectric characterization of LaAlO₃ films (thickness 90nm) spin coated from alkoxides on quartz coated with ITO, (MIM device structure, radius 250 μm). The films were annealed at 200 °C **a)** Dielectric constant vs frequency **b)** leakage current density versus applied field, **c)** Capacitance vs voltage plot (1kHz), insert shows device schematic yellow =ITO, green = LaAlO₃, red = top metal contact.

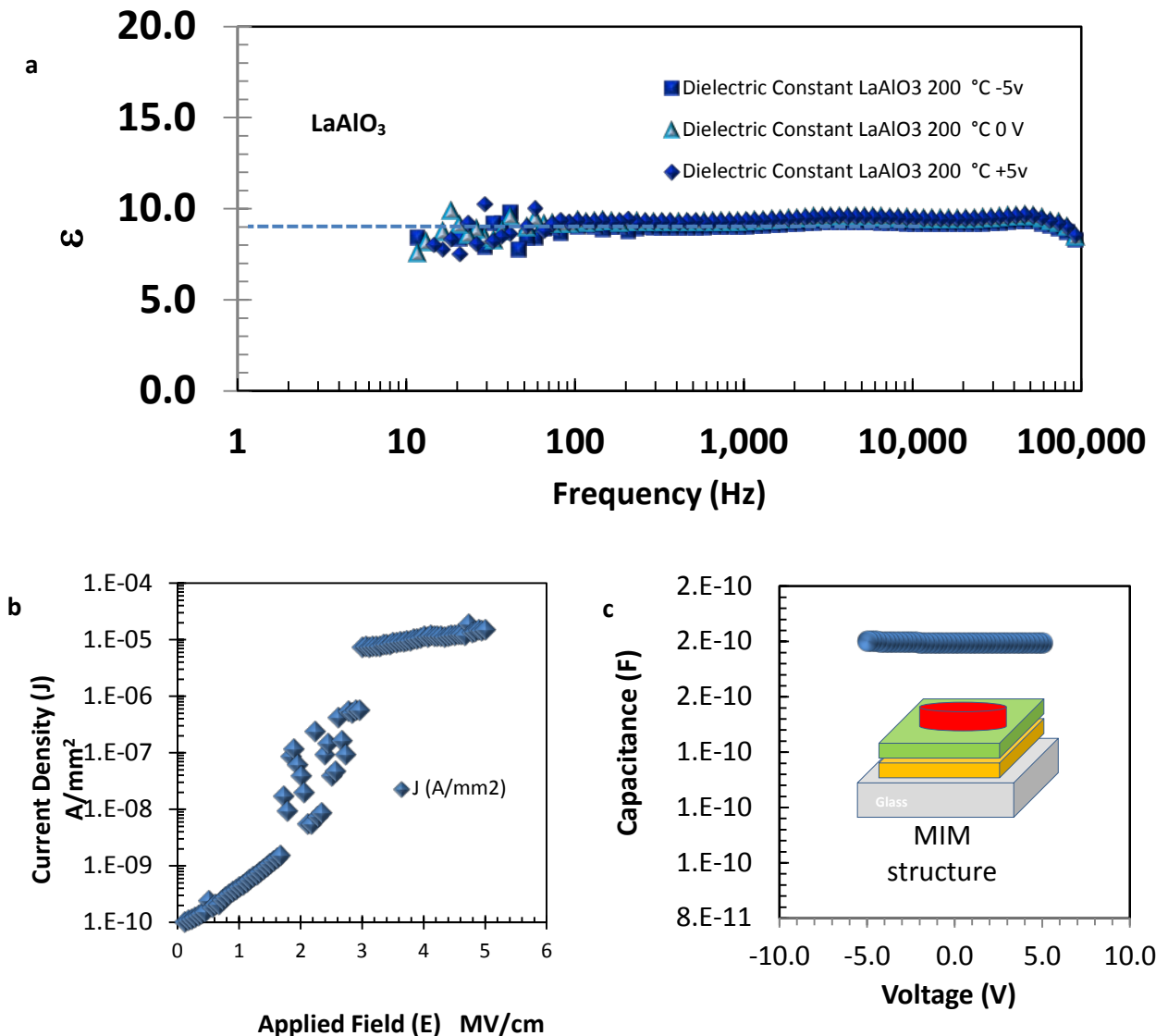


Figure S15: XPS Data for LaAlO_3 films spin coated on Si and annealed at 200 °C sample is cleaned *in situ* (500 eV for 1-2 min) to remove surface contamination. **a)** La 3d peak, **b)** 1Os peaks shows fitting for three oxygen environments (blue-O_{lattice} green-O_{vac}, and red-OH. **c)** Al 2p peak. **Table S2** Showing fitted dated from experimental analysis on La doped samples.

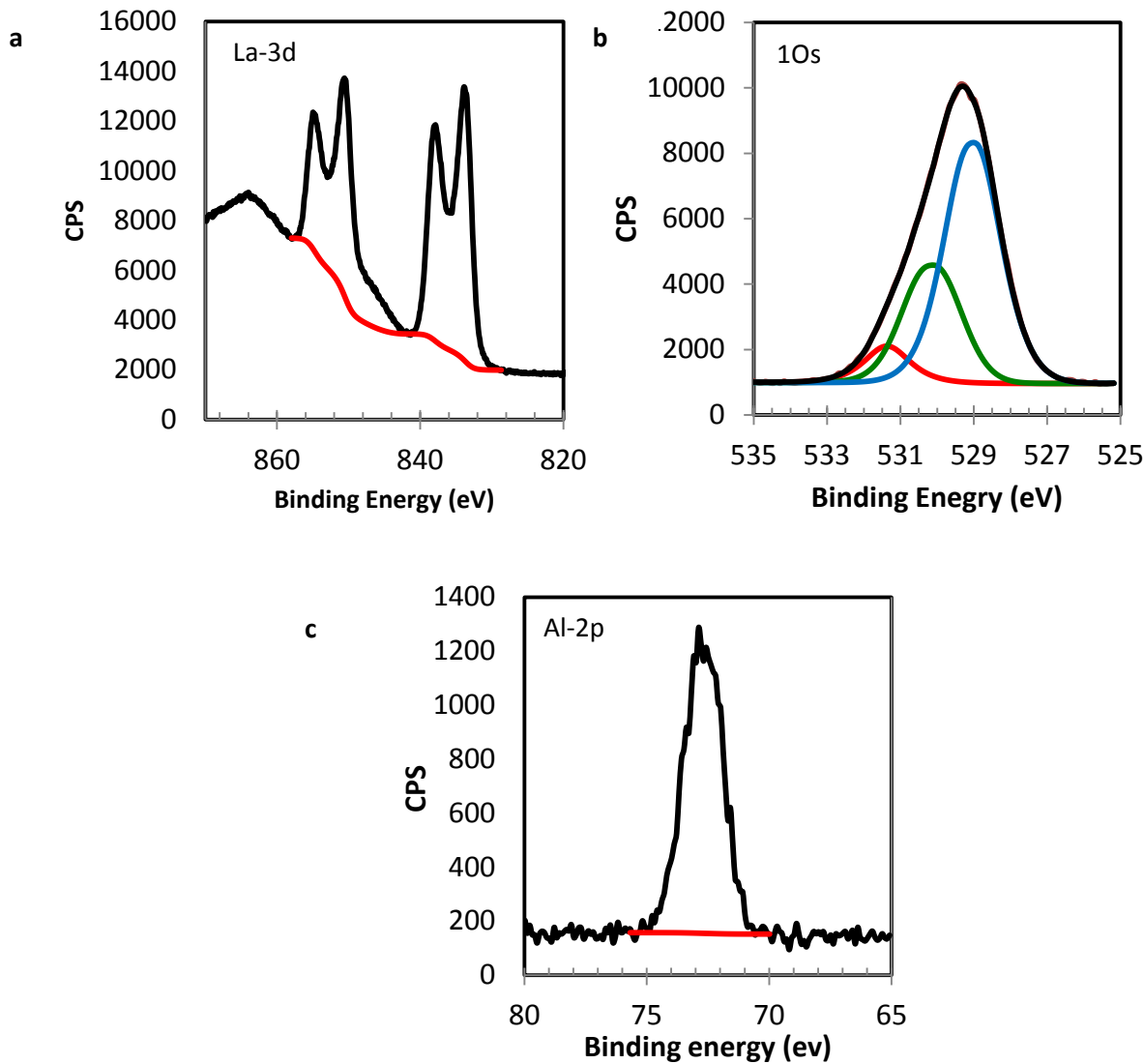


Table S2

Sample		M-OH	M-Ovac	M-Olattice	M _{Al-2p}	M _{La 3d}
LaAlO_3	BE (eV)	531.21	530.50	529.07	72.58	833.79
	FWHM	1.81	1.75	1.90	1.77	2.95
	% At	4.63	12.46	41.67	20.83	20.41

Sample		M-OH	M-O_{vac}	M-O_{lattice}	M_{Al 2p}	: M_{La 3d}
La-1.4 at%	BE (eV)	531.02	530.20	528.95	72.47	834.15
	FWHM	1.99	1.99	1.93	1.83	3.04
	% at	9.10	26.41	29.08	33.96	1.44
Sample		M-OH	M-O_{vac}	M-O_{lattice}	M_{Al 2p}	: M_{La 3d}
La 3.0 at%	BE (eV)	531.48	530.45	529.14	72.55	834.2
	FWHM	1.92	1.87	2.04	1.73	2.99
	% at	7.90	25.75	33.81	29.51	3.04
Sample		M-OH	M-O_{vac}	M-O_{lattice}	M_{Al 2p}	: M_{La 3d}
La 12.5 at%	BE (eV)	531.09	529.72	528.51	72.19	833.32
	FWHM	1.71	1.82	1.86	1.82	2.34
	% at	6.54	16.94	38.55	25.40	12.56

Figure S16 XPS depth profiling for solution processed LaAlO_3 from alkoxides. Carbon 1s peak shows presence of surface carbon plus reminder of residual carbon from sol-gel condensation as we sputter through film. Analysis of carbon content (5th cycle to negate surface contamination) shows carbon content remains largely independent with increased La doping Table S3.

Table S3	
% La doping	C 1s (%at)
La-1.4 at%	1.9
La-3.0 at%	1.7
LaAlO_3	1.9

Figure S17. C v F MIM device dielectric characterization of aqueous solution processed low temperature AlO_3 and LaAlO_3 films annealed at <275 °C prepared from metal nitrate salts dissolved in electronics grade water (thickness 145 and 90 nm respectively), (MIM device structure, radius 250 μm).

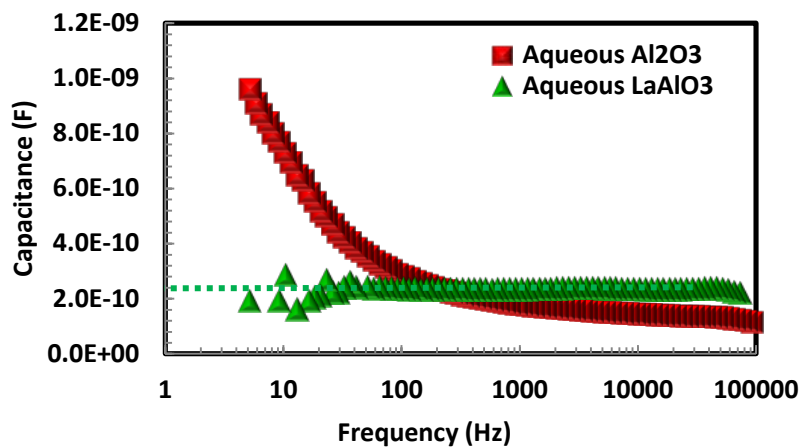


Figure S18 Forward (red) and reverse (blue) capacitance vs applied voltage plots (100Hz) for metal-insulator-semiconductor (MIS) structure with solution processed indium oxide semiconductor (20nm) and solution deposited LaAlO₃ dielectric (thickness 92nm, area $1.5 \times 10^{-6} \text{ m}^2$). Both semiconductor and dielectric films were annealed at 200 °C.

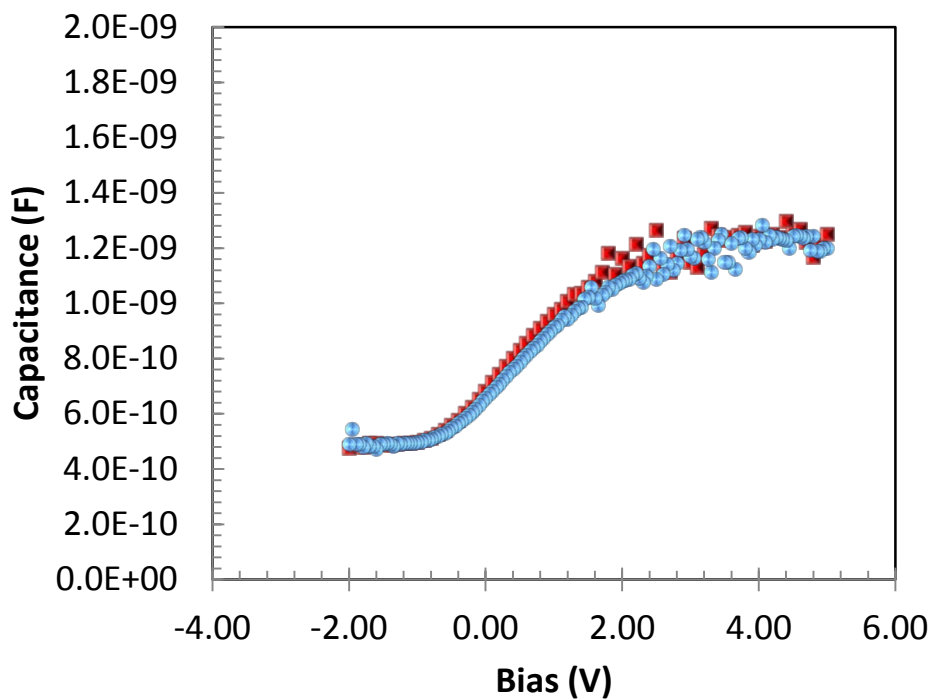


Figure S19. Statistical analysis for 42 solution processed BGTC TFTs with LaAlO_3 gate insulator (thickness 92 nm, W/L =10) and In_2O_3 semiconducting channel layer. The maximum process temperature was 200 °C.

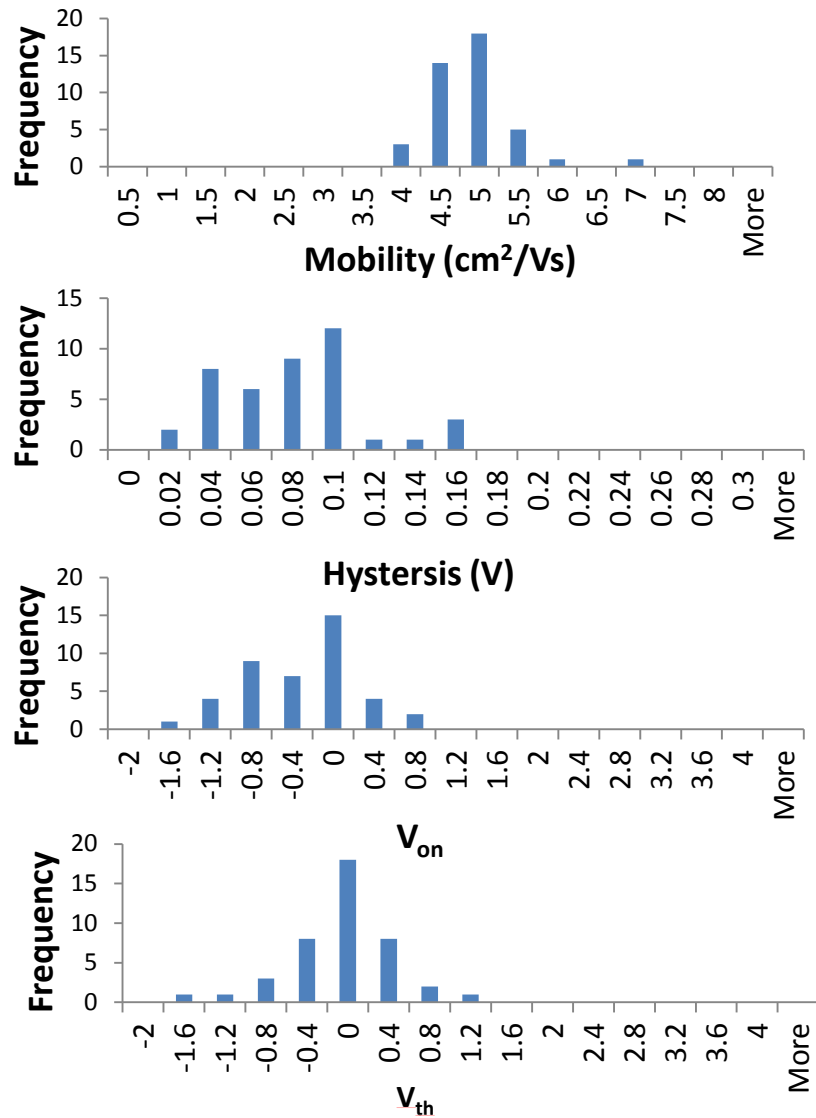


Figure S20 Main TFT parameters extracted during constant current ($5\mu\text{A}$: $\text{W}/\text{L}=10$) stress measurements as a function of stress time for solution processed $\text{LaAlO}_3 / \text{In}_2\text{O}_3$ TFTs processed at T_{\max} of 200°C .

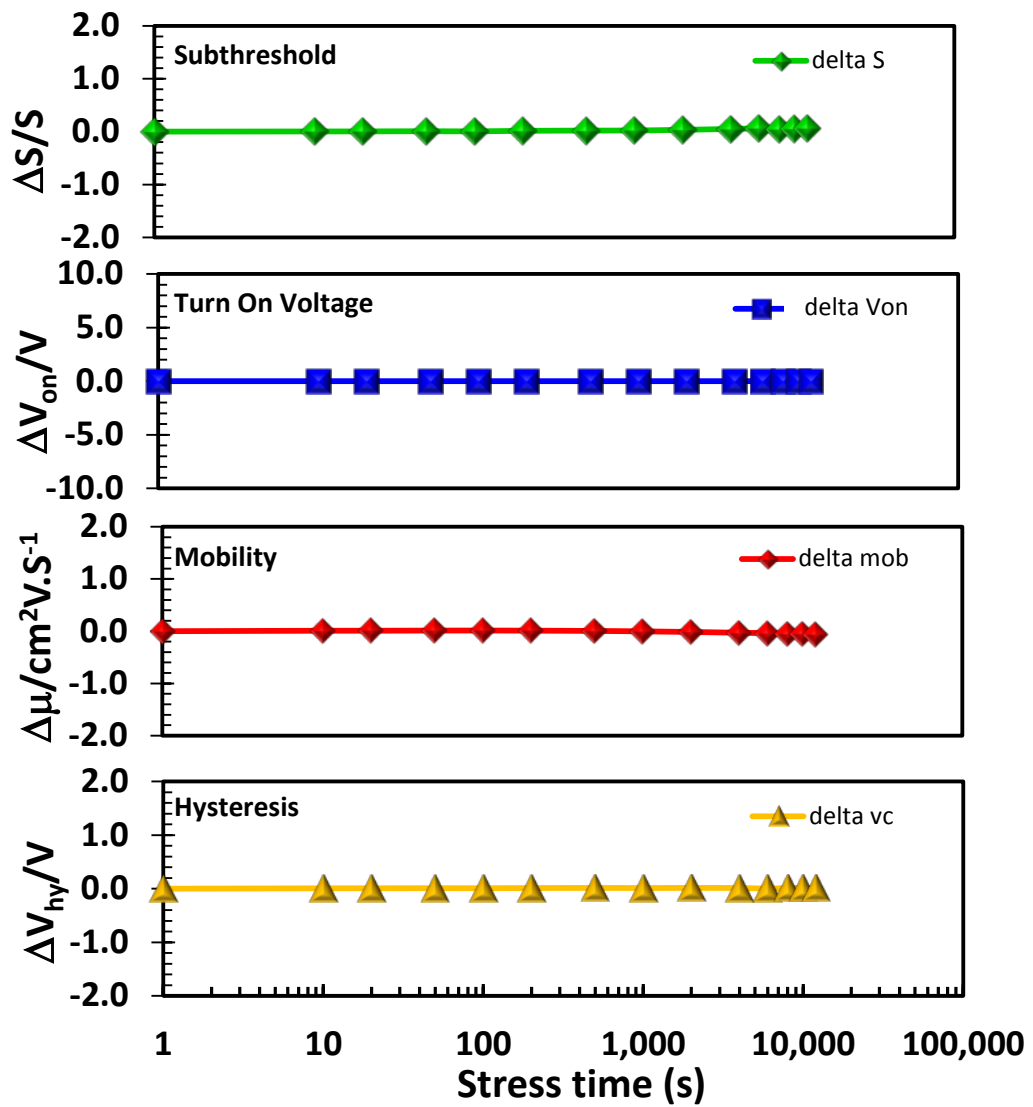


Figure S21: Solution processed hybrid transistors with organic semiconductors (max process temperature in each case is 200 °C). Hybrid TFT's were fabricated on self-assembled monolayer (SAM) surface modified solution processed La₂AlO₃ dielectric layers (92nm). The SAM surface modification used H₃PO₄ for (1-2) and octadecyltrichlorosilane (OTS) for (3), in an analogous manner as previously reported when using SiO₂ or Al₂O₃ as the dielectric layer. For the top-gate DPP-T-TT devices we spin coated a layer of LaAlO₃ on top of DPP-DTT. An orthogonal intermediate organofluorine layer (25-50nm) was first spin coated on top of DPP-DTT to avoid solvent dissolution/swelling of the underlying DPP-DTT layer. The combined stack was then annealed at 200 °C to form the LaAlO₃ dielectric layer. Optical microscopy of the hybrid stack revealed formation of hairline cracks during the annealing of the amorphous oxide layer on top of the polymer semiconductor. Hence, a layer of organic insulator (<25nm) was deposited on top of the metal oxide layer in order to prevent electrical shorting. Completed devices (W = 1000 μm , L = 20 μm) demonstrate good transistor characteristics thus illustrating that with further process optimisation our low temperature high-K dielectric may even be used as a top-gate dielectric for organic semiconductors.

